An Adaptive Finite-Difference Method for Traveltimes and Amplitudes

Jianliang Qian [*] *and William W. Symes* [†]

ABSTRACT

The point source traveltime field has an upwind singularity at the source point. Consequently, all formally high-order finite-difference eikonal solvers exhibit first-order convergence and relatively large errors. Adaptive upwind finite-difference methods based on high-order Weighted Essentially NonOscillatory (WENO) Runge-Kutta difference schemes for the paraxial eikonal equation overcome this difficulty. The method controls error by automatic grid refinement and coarsening based on an *a posteriori* error estimation. It achieves prescribed accuracy at far lower cost than does the fixed-grid method. Moreover, the achieved high accuracy of traveltimes yields reliable estimates of auxiliary quantities such as takeoff angles and geometrical spreading factors.

INTRODUCTION

Many finite-difference methods have been introduced to compute the traveltime

[*]The Rice Inversion Project, Department of Computational and Applied Mathematics, Rice University, Houston TX 77251-1892 USA, email jlqian@caam.rice.edu

[†]The Rice Inversion Project, Department of Computational and Applied Mathematics, Rice University, Houston TX 77251-1892 USA, email symes@caam.rice.edu

for isotropic media directly on regular grids (Reshef and Kosloff, 1986; Vidale, 1988; van Trier and Symes, 1991; Podvin and Lecomte, 1991; Schneider et al., 1992; Qin et al., 1992; Schneider, 1995; El-Mageed et al., 1997; Popovici and Sethian, 1997; Kim and Cook, 1999). The traveltime field is mostly smooth, suggesting that high-order finite-difference methods should be effective. The use of upwind differencing in all of the cited methods confines the errors due to singularities which develop away from the source point. The source point itself is, however, also an upwind singularity. The truncation error of a pth order method is dominated by the product of $(p+1)$st derivatives of the traveltime field and the $(p+1)$st power of the step(s). The $(p+1)$st derivatives of the traveltime field, however, behave like the $(-p+1)$th power of the distance to the source. Therefore, near the source – when the distance is on the order of the step – the truncation error is quadratic in the step, i.e., first order. This inaccuracy spreads throughout the computation and renders all higher-order methods first-order convergent. Moreover, the resultant inaccuracy in traveltime prevents reliable computation of auxiliary quantities such as takeoff angles and amplitudes.

This inaccuracy afflicts all point source traveltime computations using gridded eikonal solvers. In the few published convergence tests, implementers have resorted to imposing a grid-independent region of constant velocity near the source, in which the traveltimes are initialized analytically. This is the approach taken for instance by (Sethian, 1999) in demonstrating second-order convergence for a version of his fast marching method. This approach has two obvious drawbacks: (1) the velocity may not be homogeneous near the source; and (2) the size of the region of analytic computation must be set by the user and bears no obvious relation to the grid parameters. In principle, highly accurate ray-tracing methods could be used to alleviate the first difficulty, but the second remains: it introduces a "magic number" into the use of eikonal solvers. Kim and Cook (1999) take a different approach, similar to the one we advocate: they refine the grid several times near the source so that the reduced grid spacing compensates for the increased truncation error. However, their grid refinement strategy appears to be *ad-hoc*, and once again involves a "magic number," namely, the number of grid refinements near the source, without a clearcut selection criterion.

In this paper, we show how to use adaptive-gridding concepts commonplace in the numerical solution of ordinary differential equations (Gear, 1971) to resolve the difficulty caused by this inaccuracy. Adaptive gridding has already been used in numerical solutions of PDEs (Berger and Oliger, 1984; Berger and LeVeque, 1997). Generally, the grid refinement must be localized in several dimensions, leading to complex data structures. Fortunately, the nature of the traveltime field permits a relatively straightforward adaptive-gridding strategy introduced in (Belfi and Symes, 1998). The present work improves that of Belfi and Symes through the use of the more accurate Weighted Essentially NonOscillating (WENO) difference schemes and extends it to solutions of advection equations for various geometrical acoustics quantities. The efficiencies achieved by the adaptive gridding are considerable – usually more than an order of magnitude reduction in computation time for problems of typical exploration size, compared to fixed-grid methods giving the same level of accuracy. We also obtain dramatic improvements in the accuracy of computed geometrical acoustics quantities, such as takeoff angles and geometrical amplitudes.

The essential principle of the adaptive gridding is simple. It is based on a hierarchy of difference schemes of various orders. Presumably a higher-order step is more accurate than a lower-order step, so that the higher-order step can serve as a substitute for the exact solution in evaluating the local error in the lower-order step. Therefore, one can combine the step computations of two different orders to obtain a so-called *a posteriori* estimate of the truncation error for the lower-order step. Since the lower- and higher- order truncation errors stand in a known asymptotic relation, this permits an estimate of the higher-order truncation error as well. The asymptotic form of the truncation error then permits prediction of a step that will result in a lower-order truncation error less than a user-specified tolerance. So long as the steps are selected to maintain this local error, standard theory predicts that the higher-order global error, i.e., the actual error in the solution computed using the higher-order scheme, will be proportional to the user-specified tolerance. This straightforward idea is embedded in most modern software packages for solutions of ordinary differential equations (Gear, 1971). Its use for partial differential equations is a little more complicated because it is usually necessary to adjust the grid of the non-evolution variables along with the evolution step. As first established in (Belfi and Symes, 1998), the solution of the (paraxial) eikonal equation changes in a sufficiently predictable way to make grid adjustment practical.

The paper begins with a description of paraxial eikonal equations for traveltimes. Then we formulate the advection equation for takeoff angles and present the amplitude formulae for a two-dimensional line source and point source, respectively. We briefly describe numerical schemes needed in the adaptive-gridding approach, presenting the details in Appendices A and B. With these ingredients in place, we introduce the adaptive-gridding principle for the eikonal equation with a point source and present a simple implementation. Numerical experiments demonstrate that the new approach gives us not only accurate traveltime fields, but accurate amplitude fields as well. We conclude with some discussion on adaptive gridding in the three-dimensional case.

PARAXIAL EIKONAL EQUATIONS

The traveltime field in an isotropic solid satisfies an eikonal equation. Denote by (x_s, z_s) the coordinates of a source point, and by (x, z) the coordinates of a general point in the subsurface. The first-arrival traveltime field $\tau(x, z; x_s, z_s)$ is the viscosity solution of the eikonal equation

$$\left(\frac{\partial \tau}{\partial x}\right)^2 + \left(\frac{\partial \tau}{\partial z}\right)^2 = s^2(x, z) \tag{1}$$

with the initial condition

$$\lim \left(\frac{\tau(x,z;x_s,z_s)}{\sqrt{(x-x_s)^2+(z-z_s)^2}} - \frac{1}{v(x,z)} \right) \quad = \quad 0$$

as $(x,z) \to (x_s,z_s)$, where v is the velocity, and $s = \dfrac{1}{v}$ is the slowness (Lions, 1982).

In some seismic applications, the traveltime field is needed only in regions where

$$\frac{\partial \tau}{\partial z} \quad \geq \quad s\cos\theta_{\max} > 0,$$

i.e., along downgoing, first-arriving rays making an angle $\leq \theta_{\max} < \frac{\pi}{2}$ with the vertical. To enforce this condition, we modify the eikonal equation as an evolution equation in depth (Gray and May, 1994):

$$\frac{\partial \tau}{\partial z} = H\left(\frac{\partial \tau}{\partial x}\right) \quad = \quad \sqrt{\mathrm{smmax}\left(s^2 - \left(\frac{\partial \tau}{\partial x}\right)^2, s^2\cos^2\theta_{\max}\right)}, \tag{2}$$

where smmax is a smoothed max function, $a > 0$,

$$\mathrm{smmax}(x,a) \quad = \quad \begin{cases} \frac{1}{2}a & \text{if } x < 0, \\ \frac{1}{2}a + 2\frac{x^4}{a^3}(1 - \frac{4}{5}\frac{x}{a}) & \text{if } 0 \leq x < \frac{a}{2}, \\ x + 2\frac{(x-a)^4}{a^3}(1 + \frac{4}{5}\frac{x-a}{a}) & \text{if } \frac{a}{2} \leq x < a, \\ x & \text{if } x \geq a. \end{cases}$$

Equation (2) defines a stable nonlinear evolution in z, suitable for explicit finite-difference discretization. The smoothed max function makes the numerical Hamiltonian smooth enough to carry out standard truncation error analysis for schemes of up to third-order accuracy. The solution τ is identical to the solution of the eikonal equation provided that the ray makes an angle $\leq \theta_{\max} < \frac{\pi}{2}$ with the vertical.

ADVECTION EQUATIONS FOR TAKEOFF ANGLES

Based on the traveltime computed by solving the eikonal equation, we can approximate the amplitude field by solving a transport equation. The amplitude satisfies a transport equation (Cerveny et al., 1977):

$$\nabla \tau \cdot \nabla A + \frac{1}{2} A \nabla^2 \tau = 0. \tag{3}$$

The equation (3) is a first-order advection equation for the amplitude A. The Laplacian of the traveltime field is involved in this advection equation, which implies that we need a third-order accurate traveltime field to get a first-order accurate amplitude field (Symes, 1995; El-Mageed, 1996; El-Mageed et al., 1997).

To be convenient for the following presentation, we introduce the ray coordinates. The ray coordinates are defined by $(\tau, \phi) = (\tau(x, z; x_s, z_s), \phi(x, z; x_s, z_s))$, where τ and ϕ are the traveltime and take-off angle of a ray from source point (x_s, z_s) to a general point (x, z) in the subsurface, respectively. In two-dimensional isotropic media with line sources, the amplitude also satisfies the formula (Cerveny et al., 1977; Friedlander, 1958)

$$\begin{aligned} A &= \frac{v}{2\pi\sqrt{2}\sqrt{|J|}} \\ &= \frac{v}{2\pi\sqrt{2}}\sqrt{|\nabla \tau \times \nabla \phi|}, \end{aligned} \tag{4}$$

where $J(x, z; x_s, z_s)$ is the Jacobian of the transformation from Cartesian coordinates

(x,z) to ray coordinates (τ,ϕ). The Jacobian J can be computed by

$$J = \begin{vmatrix} \frac{\partial x}{\partial \tau} & \frac{\partial z}{\partial \tau} \\ \frac{\partial x}{\partial \phi} & \frac{\partial z}{\partial \phi} \end{vmatrix} = \begin{vmatrix} \frac{\partial \tau}{\partial x} & \frac{\partial \tau}{\partial z} \\ \frac{\partial \phi}{\partial x} & \frac{\partial \phi}{\partial z} \end{vmatrix}^{-1} = \frac{1}{\nabla\tau \times \nabla\phi}, \tag{5}$$

where $\nabla\phi$ and $\nabla\tau$ are the gradients of the takeoff angle and the traveltime, respectively.

Since the take-off angle ϕ is constant along any ray,

$$\nabla\tau \cdot \nabla\phi = \frac{\partial \tau}{\partial x}\frac{\partial \phi}{\partial x} + \frac{\partial \tau}{\partial z}\frac{\partial \phi}{\partial z} \quad = \quad 0. \tag{6}$$

That is, the wavefront normal $\nabla\tau$ is tangential to the ray; the gradient $\nabla\phi$ is tangential to the wavefront. Equation (6) is slightly easier to solve numerically than equation (3) because no second-order traveltime derivatives are explicitly involved in equation (6). Having solved equation (6) for ϕ, one produces the amplitude A through (4).

Since the typical seismic source is a point source, we need to compensate for the out-of-plane radiation in the two-dimensional (2-D) line-source amplitude formula. The 2-D amplitude with a point source (2.5-D amplitude) can be computed by

$$A \quad = \quad \frac{v}{4\pi}\sqrt{\tau_{yy}|\nabla\tau \times \nabla\phi|}, \tag{7}$$

where the out-of-plane curvature τ_{yy} satisfies another advection equation (Symes et al., 1994):

$$\frac{\partial \tau}{\partial x}\frac{\partial \tau_{yy}}{\partial x} + \frac{\partial \tau}{\partial z}\frac{\partial \tau_{yy}}{\partial z} + \tau_{yy}^2 = 0. \tag{8}$$

Supposing that the amplitude is required to be first-order accurate, the two gradients $\nabla\tau$ and $\nabla\phi$ involved in the amplitude formulae should have at least first-order accuracy. However, because $\nabla\phi$ depends on second-order derivatives of traveltime τ, it implies that to get a first-order accurate $\nabla\phi$, the traveltime τ itself should have at least third-order accuracy. The final conclusion is that a third-order traveltime solver is required to get first-order accurate amplitudes, as noted before.

Zhang (Zhang, 1993) used equation (7) in polar coordinates to compute the geometrical spreading factor, but his computation of the takeoff angle was based on the first-order traveltime field. Consequently, the gradient of take-off angle computed by his scheme was inaccurate. Vidale (Vidale and Houston, 1990) encountered a similar difficulty.

FINITE-DIFFERENCE SCHEMES

The literature suggests a large number of competing finite-difference and related schemes for the solution of the eikonal equation. We have chosen to use essentially nonoscillatory (ENO) schemes of Osher and Sethian (Osher and Sethian, 1988) and Osher and Shu (Osher and Shu, 1991) and the related weighed ENO (WENO) schemes (Liu et al., 1994; Shu, 1997; Jiang and Peng, 1997) for the following reasons: (1) stable schemes of arbitrarily high-order accuracy exist, permitting accurate solutions on coarse grids (a factor which is critical to the mesh refinement or coarsening); (2) versions exist in any dimension so that we can straightforwardly extend our methodology to the three-dimensional case (El-Mageed, 1996; El-Mageed et al., 1997; Kim and Cook, 1999).

All of these schemes take the form of recursive depth stepping rules,

$$\tau \leftarrow \tau + \delta_n^n \tau, \tag{9}$$

$$z \leftarrow z + \Delta z. \tag{10}$$

Here δ_n^n is a nonlinear update operator expressing the WENO-Runge-Kutta rule of order n, defining a difference scheme of formal nth-order accuracy and depending on Δz, Δx, and the slowness field s. Since we want to emphasize the strategy of the adaptive -gridding approach, we put the detailed form of δ_n^n $(n = 2, 3)$ in Appendix A.

Similarly, we solve the advection equation for the takeoff angle ϕ and the out-of-plane curvature τ_{yy} by using WENO schemes. See Appendix B for details.

ADAPTIVE GRIDDING IMPLEMENTATION

To initialize our algorithm, the user supplies a local error tolerance ϵ; σ_1 and σ_2 are two user-defined positive functions of ϵ which are used to control the coarsening and refinement. For example, we can take $\sigma_1 = 0.1\epsilon$ and $\sigma_2 = \epsilon$. We use the 2nd and 3rd order eikonal solvers (equations (A-1) and (A-2)) and estimate the truncation error of the 2nd-order scheme as $e_2 = \max|\delta_2^2\tau - \delta_3^3\tau|$ over the current depth. So long as $\sigma_1(\epsilon) \leq e_2 \leq \sigma_2(\epsilon)$ at every point of the current depth level, we simply proceed to the next step. It is well known and explained in Gear(1971) that an efficient adaptive stepping requires rather loose control of the local error. When $e_2 < \sigma_1(\epsilon)$, we increase the step by a factor of two, i.e., $\Delta z \leftarrow 2\Delta z$, and we recompute the τ update and e_2. Similarly, when $e_2 > \sigma_2(\epsilon)$, we decrease the step by a factor of two. As soon as the local error is once again within the tolerance interval, we continue depth-stepping. A very important point is that we retain the 3rd-order (a more accurate one) computation of τ at the end of each depth step as the actual update, discarding the 2nd-order computation, which is used only in step control.

The usual step adjustment in ODE solvers would change Δz by a factor computed from the asymptotic form of the truncation error (Stoer and Bulirsch, 1992, 449). This is impractical for a PDE application because it would require an arbitrary adjustment of the spatial grid (i.e., the x-grid in the difference scheme) and, therefore, expensive interpolation. Scaling Δz by a factor of two, however, implies that the stability may be maintained by scaling Δx by the same factor. For coarsening, this means simply throwing out every other grid point, i.e., no interpolation at all, which dramatically reduces the floating point operations required. Since the typical behaviour of the traveltime field is to become smoother as one moves away from the source, the truncation errors tend in general to decrease. Therefore, most of the grid adjustments are coarsenings and very little or no interpolation is required. Since the slowness field comes to us in gridded form, an interpolation is always required to supply estimates of slowness at the points appearing in the WENO-Runge-Kutta formula. We use a local quadratic interpolation in x and z because the third-order accuracy of which is compatible with that of the difference scheme.

Since the traveltime field is nonsmooth at the source point, the truncation error analysis on which the adaptive step selection criterion is based is not valid there. Therefore, it is necessary to produce a smooth initial traveltime field. We do this by estimating the largest $z_{\text{init}} > 0$ at which the constant velocity traveltime is in error by less than $\sigma_2(\epsilon)$. Details of the z_{init} calculation are given in Appendix C. Having initialized τ at z_{init}, the algorithm invokes adaptive gridding. Since z_{init} is quite small, τ changes rapidly, resulting in a large number of grid refinements at the outset. However, no interpolation is performed, as τ is given analytically on $z = z_{\text{init}}$. This initially very fine grid is rapidly coarsened as the depth stepping proceeds.

In our current implementation, we maintain a data structure for the computational grid that is independent of the output grid; the desired quantities are calculated on the computational grid and interpolated back to the output grid. As a safeguard against pathological program behaviors, we specify a maximum number of permitted grid refinements, MAXREF.

A simplified algorithm framework is as follows:

- Input ϵ, x_s, z_s, $\theta_{\max}$, Δz, MAXREF.
- Initialize Δx, τ, $z = z_{\text{init}}$, REF $= 0$.
- Do while $z <$ target depth,

- compute $e_2 = \max|\delta_2^2\tau - \delta_3^3\tau|$ over the current depth level z ;
- if $e_2 \leq \sigma_1(\epsilon)$ and REF > 0,
  * $\Delta z \leftarrow 2\Delta z$,
  * $\Delta x \leftarrow 2\Delta x$,
  * REF $\leftarrow$ REF $- 1$,
  * upsample τ (throw out every other point).
- else if $e_2 \geq \sigma_2(\epsilon)$ and REF $\leq$ MAXREF,
  * $\Delta z \leftarrow \Delta z/2$,
  * $\Delta x \leftarrow \Delta x/2$,
  * REF $\leftarrow$ REF $+ 1$,
  * downsample τ (interpolate)
- else
  * $z \leftarrow z + \Delta z$,
  * $\tau \leftarrow \tau + \delta_3^3\tau$.
- end if

• end do

This description leaves out the output step of the algorithm: a full implementation monitors the depth level of the next set of output points and quadratically interpolates the traveltime field onto them as soon as z passes this depth, using the current and last two depth levels of τ. Local quadratic interpolation preserves the third-order accuracy of the computed τ.

To avoid unnecessary computations, we update τ only within the triangle

$$\{(x, z) : |x - x_s| \leq |z - z_s| \tan \theta_{\max}\}.$$

All rays with takeoff angles less than $\theta_{\max}$ must lie inside this triangle, and it is only along such rays that the paraxial eikonal equation produces correct first-arrival times. Output points outside the triangle are assigned $\tau =$ MAX.FLOAT. Because traveltimes at output points which are inside the triangle but not lying on rays with takeoff angles less than $\theta_{\max}$ also receive erroneous time values, they must be washed out of any subsequent computations. For high frequency asymptotics computations, this masking is most easily accomplished by zeroing the geometrical amplitude at such points.

NUMERICAL EXPERIMENTS

To illustrate how the adaptive-gridding approach works, we test our method on a constant velocity model, $v = 1$km/s, with two-dimensional geometry $\{(x, z) : -0.5\text{km} \leq x \leq 0.5\text{km},\ 0 \leq z \leq 1.0 \text{ km}\}$, in which case the behaviors of traveltime fields and amplitude fields are well understood.

In the constant velocity case, all the desired quantities have obvious analytical solutions to compare against the computed solutions. We compare the results obtained by fixed- and adaptive- grid algorithms. Both algorithms use a third-order

WENO scheme (Appendix A) to compute τ: the adaptive-grid scheme uses a second-order ENO scheme for local truncation error estimation. The ouput grid is 51×51 with $\Delta x = \Delta z = 0.02$. For adaptive-grid algorithms, MAXREF is set to be 5 with the coarsest grid 17×17, $\sigma_1 = 0.1\epsilon$ and $\sigma_2 = \epsilon$.

Table 1 shows the traveltime error and computation cost by the fixed-grid method, and Table 2 shows the traveltime error and computation cost by the adaptive-grid method, where Flops denote the number of floating point operations. The error is the maximum absolute error at the bottom row of the gridpoints ($z = 1$km). The computed portion of this depth level (-0.5km$\leq x \leq 0.5$km) lies entirely within the computation aperture ($\theta_{\max} = 78$ degrees) and so consists of accurately computed τ values. From the two tables, we can see that to reach the same level of accuracy, the adaptive-gridding approach requires an order of magnitude lower computational cost than does the fixed-gridding approach.

Figure 1 shows the traveltime contours produced by the two approaches and we cannot see any difference between them because, on the one hand, the fixed-gridding algorithm still has first-order accuracy; on the other hand, the graphics has some visual limitation. Figure 2 shows contours of τ_x computed by two approaches. We can see that τ_x by the fixed grid is oscillating, but τ_x by the adaptive grid traveltime solver is convergent. Similar phenomena are observed for τ_z, as shown in Figure 3. Because the fixed-gridding approach gives us only first-order accurate traveltime field, the resultant traveltime derivatives have only zero-order accuracy and exhibit oscillations which do not decrease in magnitude as the grid is refined, as shown in Figure 2-Left and Figure 3-Left. However, the adaptive-gridding approach yields far more accurate traveltime fields, thus the traveltime derivatives are still accurate, as shown in Figure 2-Right and Figure 3-Right.

Now we discuss the takeoff angle and its derivatives. Figure 4 shows contours of the takeoff angle ϕ by two approaches. Because the coefficients in the advection equation for takeoff angles depend on the traveltime gradient, the accuracy of ϕ will be decided by the traveltime solver we are using. Since the first-order traveltime field from the fixed-gridding approach results in inaccurate $\nabla\tau$, the resultant takeoff angle is inaccurate, as shown in Figure 4-Left. However, the takeoff angle based on the traveltime field from the adaptive-gridding approach is accurate, as shown in Figure 4-Right. Figure 5 shows ϕ_x by the two approaches. Because the takeoff angle based on the traveltime field from the fixed-gridding approach is inaccurate, the resultant derivatives ϕ_x are divergent, as shown in Figure 5-Left. However, the adaptive-gridding approach produces accurate traveltime gradients, which leads to the convergent ϕ_x, as shown in Figure 5-Right. Similar observations hold for ϕ_z, as shown in Figure 6.

To further illustrate the differences of the accuracy between two approaches, Figures 7 and 8 show the distribution of relative errors along the depth direction for ϕ_x and ϕ_z. The error along the depth direction is defined as

$$e(z) = \frac{\max_{-0.5\le x\le 0.5}|f^{\text{comp}}(x,z) - f^{\text{ana}}(x,z)|}{\max_{-0.5\le x\le 0.5}|f^{\text{ana}}(x,z)|} \tag{11}$$

where f^{comp} is the computed solution, and f^{ana} the analytic solution. For instance, substituting f with ϕ_x in Equation (11), we get the error distribution for ϕ_x along the depth direction. From Figure 7 and Figure 8, we can conclude that the adaptive-gridding approach produces much more accurate $\nabla\phi$ than does the fixed-gridding approach. The resultant amplitudes with a line source based on $\nabla\tau$ and $\nabla\phi$ by the two approaches are shown in Figure 9; one is divergent by the fixed-gridding approach, the other accurate by the adaptive-gridding approach. Note the episodic nature of the convergence for the adaptive-gridding algorithms. Because we have allowed the local error estimate to vary by an order of magnitude before adjusting the grid and then permitted only step changes by factors of 2, the error exhibits "sticky," discontinuous behaviour.

Finally, Figure 10 shows the computational results for the out-of-plane curvature τ_{yy} and the amplitude field with the point source by adaptive-gridding approach. The computed τ_{yy} is accurate and the resultant amplitude is convergent.

We have embedded the adaptive-grid traveltime and amplitude solver in two-dimensional Kirchhoff prestack migration and inversion code (Symes et al., 1994). Figure 11 shows the impulse response of the inversion for a WENO third-order eikonal solver, where the Beylkin determinant required by the inversion is computed by using the information from traveltimes and takeoff angles.

CONCLUSIONS

In this paper first we formulated a paraxial eikonal equation with depth as evolution direction and an advection equation for takeoff angles, then we presented high-order WENO difference schemes to solve the eikonal equation for the traveltime and the advection equation for the takeoff angle. To deal with the singularity of a point source, we proposed a new adaptive-grid eikonal solver and detailed the implementation. Numerical experiments showed that the new method yields an efficiency gain of more than an order of magnitude in computational time. Adaptive gridding does not altogether eliminate the "magic number" feature, for which we criticized other approaches in the introductory section of this paper; however, our "magic number" is the local-error tolerance ϵ. In principle, the local-error tolerance ϵ is proportional to the (global) error in the computed solution, but the relation is complex (as the numerical example shows) and not a by-product of the algorithm. Nonetheless we maintain that the simplicity and homogeneity of the algorithm, and the direct if not apparent relation between ϵ and the global solution error, make the adaptive-grid scheme easier to use than its alternatives. Also, the considerable success of the variable-step selection methods for ODEs, which have the same indirect error control feature, supports this contention.

The extension to 3-D isotropic media is straightforward. Because all the difference schemes presented here can easily be extended to the three-dimensional case, there is no difficulty in implementing a 3-D version of the adaptive traveltime and amplitude solver. Moreover, we are expecting that the efficiency gain in computational cost will be even more dramatic in 3-D.

ACKNOWLEDGEMENT

The authors performed part of the research reported here while guests of the Stanford Exploration Project; JLQ and WWS thank SEP members and director Prof. Jon Claerbout for their hospitality and many stimulating discussions. JLQ thanks Dr. S. Kim for his valuable comments.

This work was partially supported by the National Science Foundation under grant number DMS 9627355, the Office of Naval Research under grant number N00014-96-1-0156, the U. S. Department of Energy under grant number DE-FG07-97 ER14827 and The Rice Inversion Project. TRIP Sponsors for 1999 are Amerada Hess, Amoco Research, Conoco Inc., Exxon Production Research Co., Geophysical Development Corporation, Landmark Graphics, Mobil, and Western Geophysical.

REFERENCES

Belfi, C. and Symes, W. W. (1998). An adaptive ENO algorithm for the eikonal equation. In *Annual Report, The Rice Inversion Project*. Rice University. (http://www.trip.caam.rice.edu/).

Berger, M. and LeVeque, R. J. (1997). Adaptive mesh refinement using wave-propagation algorithms for hyperbolic systems. In *Preprint*. Courant Institute.

Berger, M. and Oliger, J. (1984). Adaptive mesh refinement for hyperbolic partial differential equations. *J. Comput. Phys.*, 53:484–512.

Cerveny, V., Molotkov, I. A., and Psencik, I. (1977). *Ray Method in seismology.* Univerzita Karlova press.

El-Mageed, M., Kim, S., and Symes, W. W. (1997). 3-D Kirchhoff migration using finite difference traveltimes and amplitudes. In *Annual Report. The Rice Inversion Project.* Rice University. (http://www.trip.caam.rice.edu/).

El-Mageed, M. A. (1996). *3D First arrival traveltimes and amplitudes via Eikonal and Transport Finite differences solvers.* PhD thesis, Department of Computational and Applied mathematics, Rice University, Houston, TX77251-1892.

Friedlander, F. (1958). *Sound Pulses.* Cambridge University Press.

Gear, C. W. (1971). *Numerical initial value problems in ordinary differential equations.* Englewood Cliffs, N. J.: Prentice-Hall.

Gray, S. and May, W. (1994). Kirchhoff migration using eikonal equation traveltimes. *Geophysics*, 59:810–817.

Jiang, G. S. and Peng, D. P. (1997). Weighted ENO schemes for Hamilton-Jacobi equations. In *CAM97-29,UCLA.*

Jiang, G. S. and Shu, C. W. (1996). Efficient implementation of weighted ENO schemes. *J. Comput. Phys.*, 126:202–228.

Kim, S. and Cook, R. (1999). 3-D traveltime computation using second-order ENO scheme. *Geophysics*, 64:1867–1876.

Lions, P. L. (1982). *Generalized solutions of Hamilton-Jacobi equations*. Pitman Advanced Publishing Program.

Liu, X. D., Osher, S. J., and Chan, T. (1994). Weighted Essentially NonOscillatory schemes. *J. Comput. Phys.*, 115:200–212.

Osher, S. and Shu, C. W. (1991). High-order Essentially NonOscillatory schemes for Hamilton-Jacobi equations. *SIAM J. Num. Anal.*, 28:907–922.

Osher, S. J. and Sethian, J. (1988). Fronts propagating with curvature dependent speed: algorithms based on Hamilton-Jacobi formulations. *J. Comput. Phys.*, 79:12–49.

Podvin, P. and Lecomte, I. (1991). Finite difference computation of traveltimes in very contrasted velocity models: a massively parallel approach and its associated tools. *Geophys. J. Int.*, 105:271–284.

Popovici, A. M. and Sethian, J. (1997). Three-dimensional traveltime computation using the fast marching method. In *67th SEG Annual Internat. Mtg. Expanded Abstracts*, pages 1778–1781. Soc. Expl. Geophys.

Qin, F., Luo, Y., Olsen, K. B., Cai, W., and Schuster, G. T. (1992). Finite difference solution of the eikonal equation along expanding wavefronts. *Geophysics*, 57:478–487.

Reshef, M. and Kosloff, D. (1986). Migration of common shot gathers. *Geophysics*, 51:324–331.

Schneider, W. A. J. (1995). Robust and efficient upwind finite-difference traveltime calculations in three dimensions. *Geophysics*, 60:1108–1117.

Schneider, W. A. J., Ranzinger, K., Balch, A., and Kruse, C. (1992). A dynamic programming approach to first arrival traveltime computation in media with arbitrarily distributed velocities. *Geophysics*, 57:39–50.

Sethian, J. A. (1999). *Level set methods*. Cambridge Univ. Press, second edition.

Shu, C. (1997). Essentially non-oscillatory and weighted essentially non-oscillatory schemes for hyperbolic conservation laws. In *ICASE No.97-65, NASA Langley Research Center*.

Stoer, J. and Bulirsch, R. (1992). *Introduction to numerical analysis*. Springer-Verlag, New York, second edition.

Symes, W. W. (1995). Mathematics of reflection seismology. In *Annual Report, The Rice Inversion Project*. Rice University. (http://www.trip.caam.rice.edu/).

Symes, W. W., Versteeg, R., Sei, A., and Tran, Q. H. (1994). Kirchhoff simulation, migration and inversion using finite difference traveltimes and amplitudes. In *Annual Report, The Rice Inversion Project*. Rice University. (http://www.trip.caam.rice.edu/).

van Trier, J. and Symes, W. W. (1991). Upwind finite-difference calculation of traveltimes. *Geophysics*, 56:812–821.

Vidale, J. (1988). Finite-difference calculation of travel times. *Bull., Seis. Soc. Am.*, 78:2062–2076.

Vidale, J. E. and Houston, H. (1990). Rapid calculation of seismic amplitudes. *Geophysics*, 55:1504–1507.

Zhang, L. (1993). *Imaging by the wavefront propagation method.* PhD thesis, Stanford University, Stanford, CA94305.

Appendix A. ENO AND WENO SCHEMES FOR EIKONAL EQUATION

Our adaptive scheme is based on the second- and third- order WENO difference schemes introduced by Jiang and Peng (Jiang and Peng, 1997). These are in turn extensions of second- and third-order ENO difference schemes, which we present first.

For a function f of the space variable (x, z) in the computational domain, we write

$$\begin{aligned} f_i^k &= f(x_i, z_k), \\ (x_i, z_k) &= (x_{\min} + (i-1)\Delta x, z_{min} + (k-1)\Delta z). \end{aligned}$$

Let

$$\tau_i^k = \tau(x_i, z_k; x_s, z_s)$$

and define the forward D^+ and backward D^- finite-difference operators

$$D_x^\pm \tau_i^k = \frac{\pm[\tau_{i\pm 1}^k - \tau_i^k]}{\Delta x}.$$

The second- and third-order ENO refinements of $D_x^\pm \tau$ are

$$\begin{aligned} D_x^{\pm,2}\tau_i &= D_x^\pm \tau_i \mp \frac{1}{2}\Delta x\ m(D_x^\pm D_x^\pm \tau_i, D_x^- D_x^+ \tau_i), \\ D_x^{\pm,3}\tau_i &= D_x^{\pm,2}\tau_i - \frac{1}{6}(\Delta x)^2\ m(D_x^\pm D_x^\pm D_x^\pm \tau_i, D_x^+ D_x^+ D_x^- \tau_i, D_x^+ D_x^- D_x^- \tau_i), \end{aligned}$$

where

$$m(x,y) = \min(\max(x,0), \max(y,0)) + \max(\min(x,0), \min(y,0)).$$

Similar refinements exist of any order.

The upwind ENO approximations for $\frac{\partial \tau}{\partial x}$ are

$$\widehat{D}_x^n \tau = \text{modmax}(\max(D_x^{-,n}\tau, 0), \min(D_x^{+,n}\tau, 0)),$$

where the modmax function returns the larger value in modulus.

The second-order and third-order ENO Runge-Kutta steps are

$$\begin{aligned} \delta_2^1 \tau &= \Delta z H(\widehat{D}_x^2 \tau), \\ \delta_2^2 \tau &= \frac{1}{2}\left(\delta_2^1 \tau + \Delta z H(\widehat{D}_x^2(\tau + \delta_2^1 \tau))\right), \end{aligned} \qquad \text{(A-1)}$$

and

$$\begin{aligned}
\delta_3^1\tau &= \Delta z H(\widehat{D}_x^3\tau), \\
\delta_3^2\tau &= \frac{1}{4}\left(\delta_3^1\tau + \Delta z H(\widehat{D}_x^3(\tau+\delta_3^1\tau))\right), \\
\delta_3^3\tau &= \frac{1}{3}\left(2\delta_3^2\tau + 2\Delta z H(\widehat{D}_x^3(\tau+\delta_3^2\tau))\right).
\end{aligned} \tag{A-2}$$

The depth step Δz must satisfy the stability condition

$$\Delta z \le \Delta z_{\rm cfl} = \frac{\Delta x}{\tan(\theta_{\rm max})}.$$

We have typically chosen $\Delta z = 0.9\Delta z_{\rm cfl}$.

The nth-order scheme is then

$$\tau^{k+1} = \tau^k + \delta_n^n\tau^k \tag{A-3}$$

for $k = 0, 1, 2, \cdots$.

We have observed that the gradient of the take-off angle based on the third-order ENO traveltime is too noisy to lead to an accurate amplitude field. To alleviate this phenomenon, instead of ENO third-order refinements, we use WENO third-order refinement (Jiang and Peng, 1997) to compute $D_x^\pm\tau$ in the third-order Runge-Kutta step, which yields an accurate amplitude field.

The WENO third-order schemes for $D_x^\pm\tau_i$ are

$$\begin{aligned}
D_x^{\pm\mathrm{W},3}\tau_i &= \frac{1}{12}\left(-D_x^+\tau_{i-2} + 7D_x^+\tau_{i-1} + 7D_x^+\tau_i - D_x^+\tau_{i+1}\right) \\
&\pm \Delta x\Phi^{\mathrm{WENO}}\left(D_x^-D_x^+\tau_{i\pm2}, D_x^-D_x^+\tau_{i\pm1}, D_x^-D_x^+\tau_i, D_x^-D_x^+\tau_{i\mp1}\right),
\end{aligned}$$

where

$$\Phi^{\mathrm{WENO}}(a,b,c,d) = \frac{1}{3}w_0(a-2b+c)+\frac{1}{6}(w_2-\frac{1}{2})(b-2c+d)$$

with weights defined as

$$\begin{aligned}
w_0 &= \frac{\alpha_0}{\alpha_0+\alpha_1+\alpha_2}, w_2 = \frac{\alpha_2}{\alpha_0+\alpha_1+\alpha_2}, \\
\alpha_0 &= \frac{1}{(\delta+\beta_0)^2}, \alpha_1 = \frac{1}{(\delta+\beta_1)^2}, \alpha_2 = \frac{1}{(\delta+\beta_2)^2}, \\
\beta_0 &= 13(a-b)^2+3(a-3b)^2, \\
\beta_1 &= 13(b-c)^2+3(b+c)^2, \\
\beta_2 &= 13(c-d)^2+3(3c-d)^2.
\end{aligned}$$

In the denominators above, we added a small positive number δ to avoid dividing by zero.

Appendix B. WENO SCHEMES FOR ADVECTION EQUATIONS

Recall the advection equation for the takeoff angle,

$$\frac{\partial\tau}{\partial x}\frac{\partial\phi}{\partial x}+\frac{\partial\tau}{\partial z}\frac{\partial\phi}{\partial z} = 0. \tag{B-1}$$

To match with the evolution form of the eikonal equation in depth, we formulate the advection equation as an evolution equation in depth as well, i.e.,

$$\frac{\partial\phi}{\partial z} = -\left(\frac{\partial\tau}{\partial z}\right)^{-1}\frac{\partial\tau}{\partial x}\frac{\partial\phi}{\partial x}. \tag{B-2}$$

To fully take advantage of the accuracy of traveltimes produced by the WENO Runge-Kutta third-order scheme for the eikonal equation and simplify the implementation, we embed the third-order scheme for equation (B-2) into the third-order scheme for the eikonal equation.

At first, we introduce the approximations for x-derivative and z-derivative of τ in the above advection equation:

$$\frac{\partial \tau}{\partial x} \approx D_x[\tau] \quad = \quad \max(D_x^{-\mathrm{W},3}\tau, 0) + \min(D_x^{+\mathrm{W},3}\tau, 0), \tag{B-3}$$

$$\frac{\partial \tau}{\partial z} \quad \approx \quad H(\widehat{D_x^3}\tau). \tag{B-4}$$

Next, we define the upwind difference approximation for $\frac{\partial \phi}{\partial x}$. Because the choice of stencil in ENO schemes is too sensitive to the zeros of solution (Liu et al., 1994; Jiang and Shu, 1996), we use WENO schemes to approximate the derivative $\frac{\partial \phi}{\partial x}$.

Because the coefficient of the discretized advection equation has only second-order accuracy, which is computed from the eikonal equation by third-order scheme, we use a second-order WENO scheme to approximate the derivatives $\frac{\partial \phi}{\partial x}$. The second-order WENO scheme is based on the second-order ENO stencils, so it does not give rise to any new complexities in the coding.

The second-order upwind WENO approximations to $\frac{\partial \phi}{\partial x}$ (Jiang and Peng, 1997) are

$$\begin{aligned}
(\frac{\partial \phi}{\partial x})_i^k \approx (D_x^{-\mathrm{W},2}\phi)_i^k \quad &= \quad \frac{1}{2}(D_x^+\phi_{i-1}^k + D_x^+\phi_i^k) - \frac{w_-}{2}(D_x^+\phi_{i-2}^k - 2D_x^+\phi_{i-1}^k + D_x^+\phi_i^k), \\
(\frac{\partial \phi}{\partial x})_i^k \approx (D_x^{+\mathrm{W},2}\phi)_i^k \quad &= \quad \frac{1}{2}(D_x^+\phi_{i-1}^k + D_x^+\phi_i^k) - \frac{w_+}{2}(D_x^+\phi_{i+1}^k - 2D_x^+\phi_i^k + D_x^+\phi_{i-1}^k),
\end{aligned}$$

where

$$w_- = \frac{1}{1+2r_-^2}, \qquad r_- = \frac{\delta + (D_x^- D_x^- \phi_i^k)^2}{\delta + (D_x^- D_x^+ \phi_i^k)^2},$$
$$w_+ = \frac{1}{1+2r_+^2}, \qquad r_+ = \frac{\delta + (D_x^+ D_x^+ \phi_i^k)^2}{\delta + (D_x^- D_x^+ \phi_i^k)^2},$$

and δ is a small positive constant to avoid the denominators from becoming zero.

Now we define the upwind WENO difference for $\frac{\partial \phi}{\partial x}$ which corresponds to the upwind direction of $\frac{\partial \tau}{\partial x}$ as follows:

$$D_x^{\text{up}} \phi_i^k = \begin{cases} D_x^{-\text{W},2} \phi_i^k & \text{if } D_x[\tau]_i^k \geq 0, \\ D_x^{+\text{W},2} \phi_i^k & \text{else.} \end{cases} \tag{B-5}$$

Finally we can formulate the third-order WENO Runge-Kutta scheme for the advection equation as

$$\begin{aligned} \delta_3^1 \phi &= \Delta z \Psi(\widehat{D}_x^3 \tau, \phi), \\ \delta_3^2 \phi &= \frac{1}{4}\left(\delta_3^1 \phi + \Delta z \Psi(\widehat{D}_x^3(\tau + \delta_3^1 \tau), \phi + \delta_3^1 \phi)\right), \\ \delta_3^3 \phi &= \frac{1}{3}\left(2\delta_3^2 \phi + 2\Delta z \Psi(\widehat{D}_x^3(\tau + \delta_3^2 \tau), \phi + \delta_3^2 \phi)\right), \end{aligned} \tag{B-6}$$

where

$$\Psi(\tau, \phi) = -\frac{D_x[\tau] D_x^{up} \phi}{H(\widehat{D}_x^3(\tau))}. \tag{B-7}$$

The third-order scheme for ϕ is then

$$\phi^{k+1} = \phi^k + \delta_3^3 \phi^k \tag{B-8}$$

for $k = 0, 1, 2, \cdots$. But this scheme is really a second-order scheme, because the coefficients have only second-order accuracy.

With a few changes, we can modify the above scheme for the takeoff angle to solve the advection equation for τ_{yy}.

Appendix C. ESTIMATE THE INITIAL STEP

To initialize the traveltime for finite-difference schemes, we assumed that the velocity near the source is constant and equal to the source velocity. Now we desire to analyse the traveltime error caused by this assumption and furthermore compute an *a priori* estimate of the initial step.

Assuming that the source is at origin, we consider the two-dimensional ray-tracing equation. By the method of characteristics, we have

$$\dot{x} = v^2 p, \tag{C-1}$$

$$\dot{z} = v^2 q, \tag{C-2}$$

$$\dot{p} = -\frac{1}{v}\frac{\partial v}{\partial x}, \tag{C-3}$$

$$\dot{q} = -\frac{1}{v}\frac{\partial v}{\partial z}, \tag{C-4}$$

where the dot $\cdot$ denotes the differentiation with respect to time t along the ray; $p = \dfrac{\partial \tau}{\partial x}$ and $q = \dfrac{\partial \tau}{\partial z}$.

Denote the group angle as θ, then we have

$$\dot{x} = v \sin\theta, \tag{C-5}$$

$$\dot{z} = v \cos\theta; \tag{C-6}$$

furthermore, equations (C-1) and (C-2) yield

$$p = \frac{\sin\theta}{v(x,z)}, \tag{C-7}$$

$$q = \frac{\cos\theta}{v(x,z)}. \tag{C-8}$$

Differentiate equation (C-7) with respect to time t and simplify the resultant equation, then we have

$$\dot{\theta} = -\cos\theta\frac{\partial v}{\partial x} + \sin\theta\frac{\partial v}{\partial z}. \tag{C-9}$$

Now we introduce polar coordinates, i.e.

$$x = r\sin\psi, \tag{C-10}$$

$$z = r\cos\psi. \tag{C-11}$$

Differentiating equations (C-10) and (C-11) with respect to time t and solving for $\dot{r}$ and $\dot{\psi}$, we have

$$\dot{r} = v\cos(\theta-\psi), \tag{C-12}$$

$$\dot{\psi} = \frac{v}{r}\sin(\theta-\psi). \tag{C-13}$$

Next we want to estimate $(\theta-\psi)$. First of all, we have $|\theta-\psi|<\pi$, since for the downward wave propagation both θ and ψ lie in the interval $(-\frac{\pi}{2},\frac{\pi}{2})$. Define

$$a(t) = \dot{\theta}, \tag{C-14}$$

$$b(t) = \frac{vt}{r}\frac{\sin(\theta-\psi)}{(\theta-\psi)}, \tag{C-15}$$

then by (C-9) and (C-13) we have an ordinary differential equation for $(\theta - \psi)$,

$$\dot{\theta} - \dot{\psi} = a(t) - \frac{b(t)}{t}(\theta - \psi). \qquad \text{(C-16)}$$

Its solution is

$$\theta - \psi = \int_0^t d\tau a(\tau) \exp\left(-\int_\tau^t d\sigma \frac{b(\sigma)}{\sigma}\right). \qquad \text{(C-17)}$$

Because $b(t) \geq 0$ and the function a is bounded by $a_{\max}$, which is equal to the supremum of the length of gradient of the velocity, i.e., $|a| \leq a_{\max}$, equation (C-17) yields an estimate for $\theta - \psi$,

$$|\theta - \psi| \leq a_{\max} t. \qquad \text{(C-18)}$$

Now we are ready to get an approximate relative error estimate for the traveltime. Denote t_0 as the approximation to the exact traveltime t when we are using the constant velocity v_0 at the source as the approximation to the exact velocity v. Since

$$\dot{t_0} = \frac{\dot{r}}{v_0} = \frac{v}{v_0}\cos(\theta - \psi), \qquad \text{(C-19)}$$

we have

$$\dot{t_0} - \dot{t} = \left(\frac{v}{v_0} - 1\right)\cos(\theta - \psi) + \cos(\theta - \psi) - 1; \qquad \text{(C-20)}$$

furthermore,

$$|\dot{t_0} - \dot{t}| \leq \left|\frac{v}{v_0} - 1\right| + |\cos(\theta - \psi) - 1|. \qquad \text{(C-21)}$$

Noticing that if $|\dot{t_0} - \dot{t}| \le \varepsilon$, then $|t_0 - t| \le \varepsilon t$. So let's specify that

$$\left|\frac{v}{v_0} - 1\right| \le \frac{\varepsilon}{2} \tag{C-22}$$

and

$$|\cos(\theta - \psi) - 1| \le \frac{\varepsilon}{2}. \tag{C-23}$$

Expanding v at the origin (the source) by Taylor theorem with remainder, we have

$$v(x,z) = v_0 + \frac{\partial v}{\partial x}(\zeta_1, \eta_1)x + \frac{\partial v}{\partial z}(\zeta_2, \eta_2)z, \tag{C-24}$$

where (ζ_1, η_1) and (ζ_2, η_2) lie in

$$D = \{(\zeta, \eta) : \min(x, 0) \le \zeta \le \max(x, 0), 0 \le \eta \le z\}. \tag{C-25}$$

As a consequence,

$$|v(x,z) - v_0| \le \sqrt{2}r \sup\{|\nabla v(\zeta, \eta)| : |\zeta| \le |x|, 0 \le \eta \le z\} \tag{C-26}$$

by Cauchy inequality.

Because we are only bounding the error inside the aperture,

$$|x| \le z \tan\theta_{\max}, \qquad r \le \frac{z}{\cos\theta_{\max}}; \tag{C-27}$$

it follows that

$$\begin{aligned}
\left|\frac{v - v_0}{v_0}\right| &\le \frac{\sqrt{2}r}{v_0} \sup\{|\nabla v(\zeta, \eta)| : |\zeta| \le z \tan\theta_{\max}, 0 \le \eta \le z\} \\
&\le \frac{\sqrt{2}r}{v_0} \sup\{|\nabla v(\zeta, \eta)| : |\zeta| \le z_{\max} \tan\theta_{\max}, 0 \le \eta \le z_{\max}\} \\
&\le \frac{\sqrt{2}zB}{v_0 \cos\theta_{\max}},
\end{aligned} \tag{C-28}$$

where $z_{\max}$ is the maximum depth and

$$B = \sup\{|\nabla v(\zeta,\eta)| : |\zeta| \le z_{\max}\tan\theta_{\max}, 0 \le \eta \le z_{\max}\}. \tag{C-29}$$

For (C-22) to hold, by (C-28) we should choose z such that

$$z \le z_1 = \frac{v_0 \varepsilon \cos\theta_{\max}}{2\sqrt{2}B}. \tag{C-30}$$

Finally we choose z so that (C-23) holds, and we need a lemma to do so.

Lemma 1: *Along a ray segment $\{(x(\tau), z(\tau)) : 0 \le \tau \le t\}$, the following inequality holds:*

$$t \le \frac{r}{v_{\min}}, \tag{C-31}$$

where $r = \sqrt{x^2(t) + z^2(t)}$; $v_{\min}$ is the minimum velocity along the ray segment.

Proof Denote the true ray path as s and its length $|s|$, and the straight ray path as l and its length $|l|$ which is equal to r. In addition, we are using l to approximate the true ray path s. Then by Fermat's principle, we have

$$t = \int_s d\sigma \frac{1}{v} \le \int_l d\sigma \frac{1}{v} \le \int_l d\sigma \frac{1}{v_{\min}} = \frac{r}{v_{\min}}. \tag{C-32}$$

Using (C-18) and **Lemma 1**, we have

$$\begin{aligned} |\cos(\theta - \psi) - 1| &= \left| -2\sin^2\frac{(\theta-\psi)}{2} \right| \\ &\le \frac{(\theta-\psi)^2}{2} \\ &\le \frac{r^2 a_{\max}^2}{v_{\min}^2} \\ &\le \frac{r^2 B^2}{v_{\min}^2}, \end{aligned} \tag{C-33}$$

where we have used the relation $a_{\max} \leq B$ inside the aperture. Hence to make (C-23) hold implies that

$$z \leq z_2 \quad = \quad \sqrt{\frac{\varepsilon}{2}} \frac{v_{\min} \cos \theta_{\max}}{B}. \tag{C-34}$$

So for error tolerance ε, z_{init} should be chosen such that

$$z_{\text{init}} \quad = \quad \min (z_1, z_2). \tag{C-35}$$

Although both z_1 and z_2 depend on B (the bound of gradient of velocity model), there are at least two ways to estimate B. One way is simply setting B to be a big number which is larger than the actual value; the other way is computing the gradient of velocity model from the given discretized model. Both ways will produce a reasonable initial step.

Captions and Headings

Table 1. Fixed-grid eikonal solver: a constant velocity model.

Table 2. Adaptive-grid eikonal solver: a constant velocity model.

Figure 1. Traveltime contours for a constant velocity model. Left: fixed grid. Right: adaptive grid.

Figure 2. τ_x for a constant velocity model. Left: τ_x by fixed grid is oscillating. Right: τ_x by adaptive grid is convergent.

Figure 3. τ_z for a constant velocity model. Left: τ_z by fixed grid is oscillating. Right: τ_z by adaptive grid is convergent.

Figure 4. Takeoff angle ϕ for a constant velocity model. Left: ϕ by fixed grid is not accurate enough to be differentiated. Right: ϕ by adaptive grid is accurate enough to be differentiated.

Figure 5. ϕ_x at $z = 1$ for a constant velocity model. Left: fixed grid; solid line (-): true solution; star (*): computed solution. Right: adaptive grid; solid line (-): true solution; star (*): computed solution.

Figure 6. ϕ_z at $z = 1$ for a constant velocity model. Left: fixed grid; solid line (-): true solution; star (*): computed solution. Right: adaptive grid; solid line (-): true solution; star (*): computed solution.

Figure 7. Relative errors in ϕ_x. Left: fixed grid, maximum relative error is almost 45 percent. Right: adaptive grid, maximum relative error is less than 1.5

percent.

Figure 8. Relative errors in ϕ_z. Left: fixed grid, maximum relative error is almost 30 percent. Right: adaptive grid, maximum relative error is less than 1.5 percent.

Figure 9. 2-D amplitude with line source for a constant velocity model. Left: the amplitude by fixed grid is divergent. Right: the amplitude by adaptive grid is convergent.

Figure 10. Left: τ_{yy} at $z = 1$ for a constant velocity model by adaptive grid; solid line (-): true solution; star (*): computed solution. Right: 2D amplitude with point source for a constant velocity model by adaptive grid.

Figure 11. The impulse response by inversion with adaptive-gridding WENO traveltime-amplitude solver. The Beylkin determinant needed in the inversion is computed by using the information from traveltimes and takeoff angles, and the response is smooth as expected.

dx	Abs.Err(τ, dx)(s)	$Flops$
0.01	0.001232	261,590
0.00125	0.000219	16,632,765

Table 1. Fixed-grid eikonal solver: a constant velocity model

ϵ	Abs.Err(τ, dx)(s)	$Flops$
0.000025	0.001041	39,815
0.00000169	0.000160	928,770

Table 2. Adaptive-grid eikonal solver: a constant velocity model

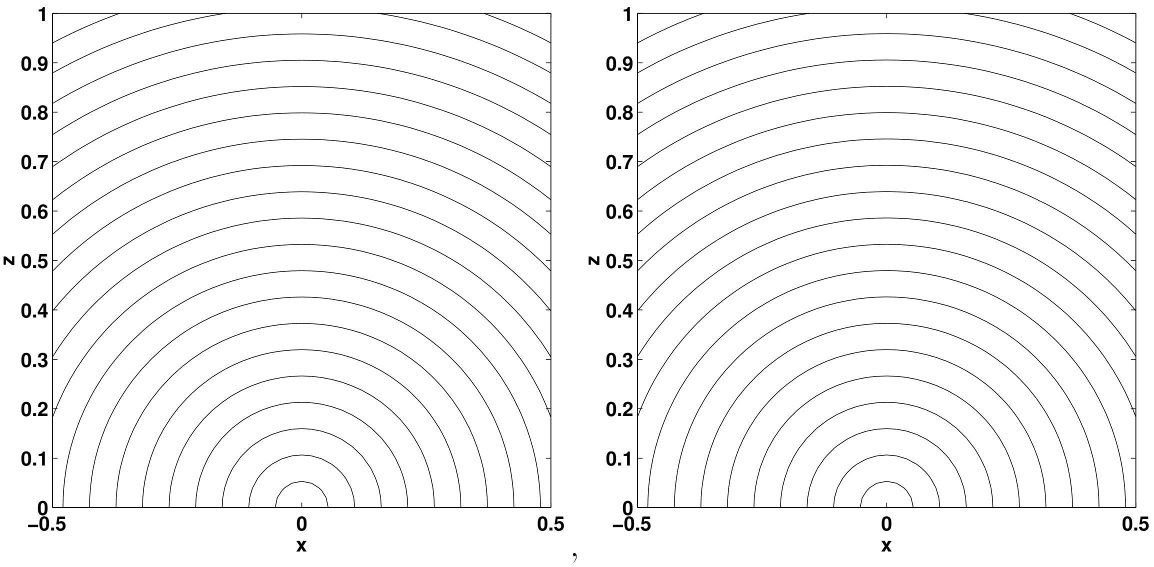

FIG. 1. Traveltime contours for a constant velocity model. Left: fixed grid. Right: adaptive grid.

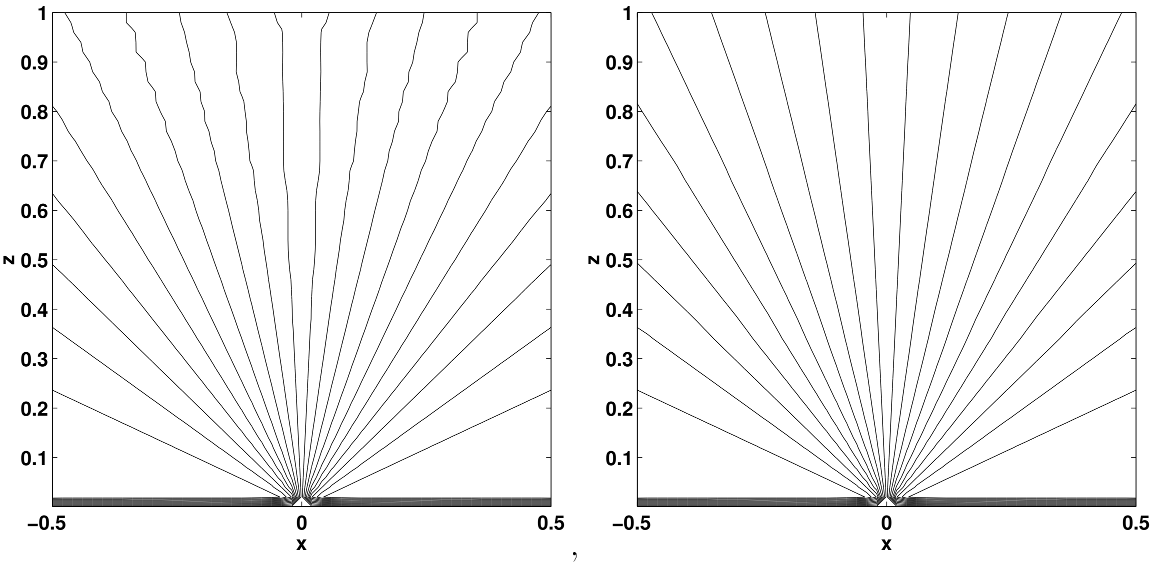

FIG. 2. τ_x for a constant velocity model. Left: τ_x by fixed grid is oscillating. Right: τ_x by adaptive grid is convergent.

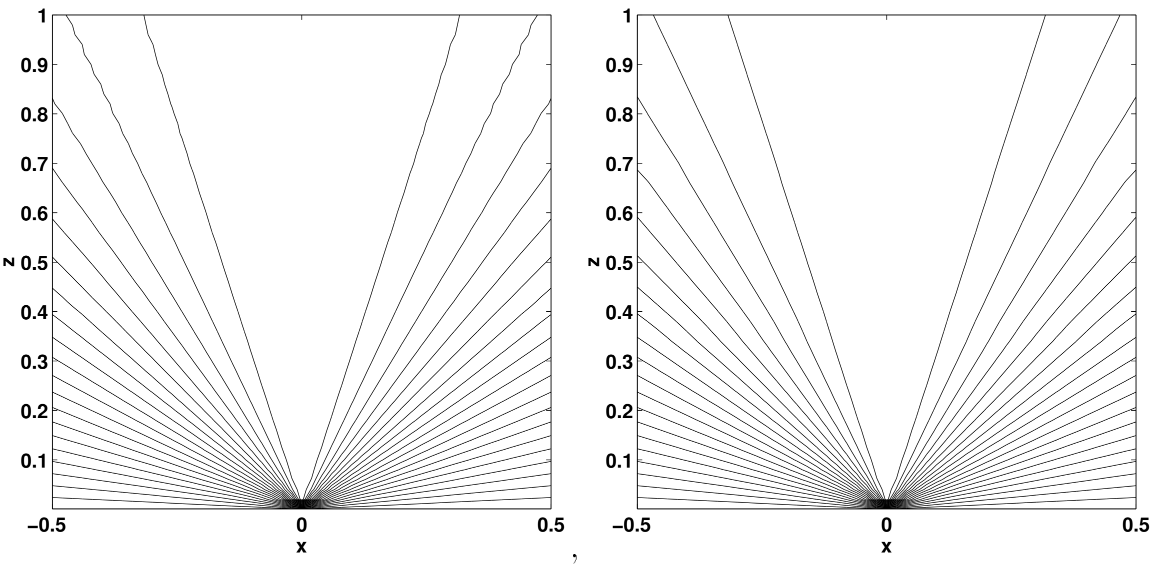

FIG. 3. τ_z for a constant velocity model. Left: τ_z by fixed grid is oscillating. Right: τ_z by adaptive grid is convergent.

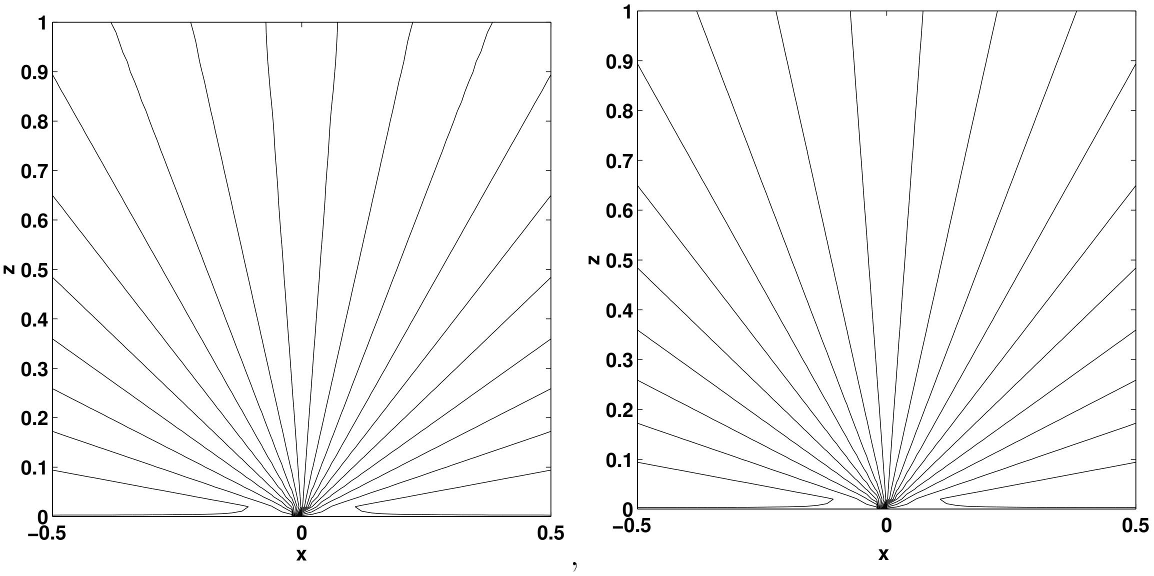

FIG. 4. Takeoff angle ϕ for a constant velocity model. Left: ϕ by fixed grid is not accurate enough to be differentiated. Right: ϕ by adaptive grid is accurate enough to be differentiated.

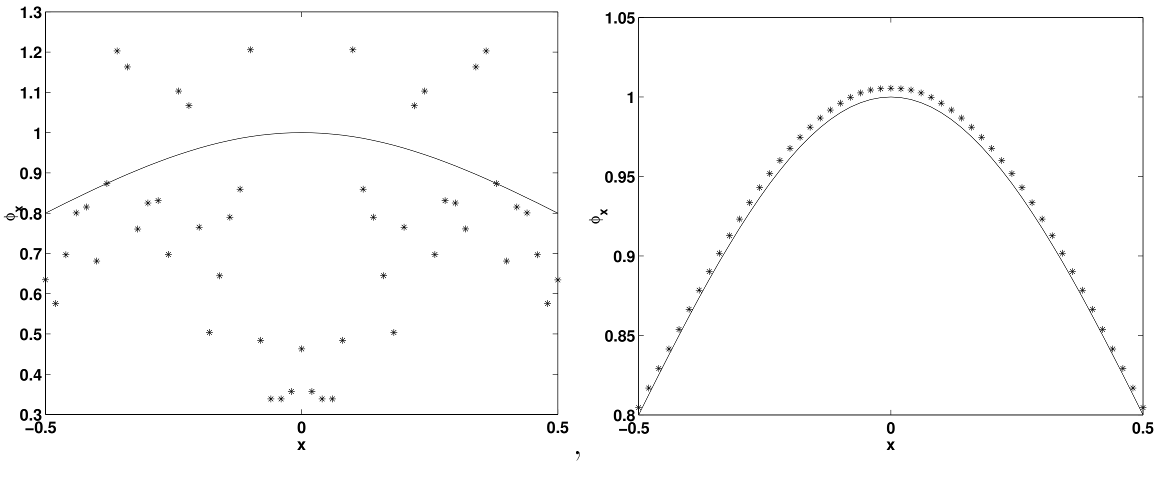

FIG. 5. ϕ_x at $z = 1$ for a constant velocity model. Left: fixed grid; solid line (-): true solution; star (*): computed solution. Right: adaptive grid; solid line (-): true solution; star (*): computed solution.

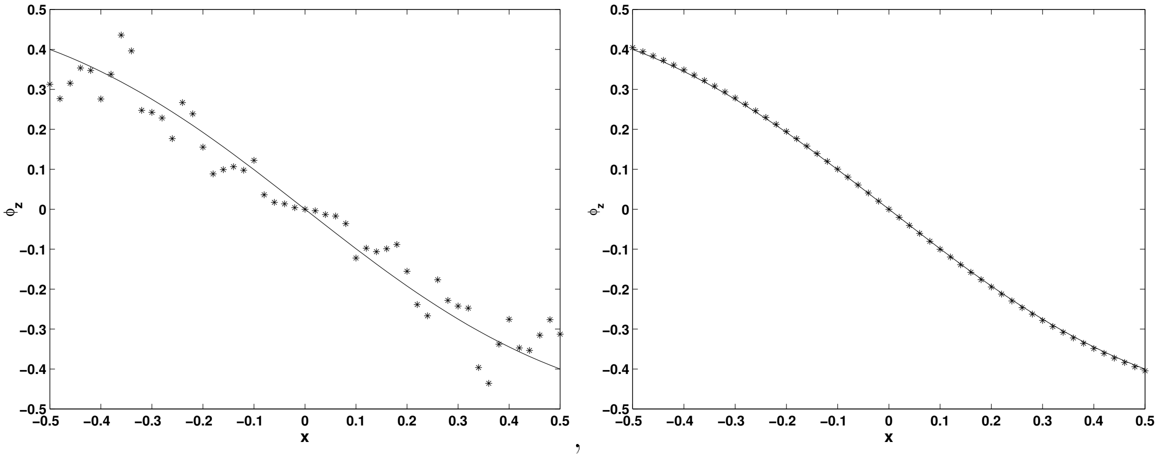

FIG. 6. ϕ_z at $z = 1$ for a constant velocity model. Left: fixed grid; solid line (-): true solution; star (*): computed solution. Right: adaptive grid; solid line (-): true solution; star (*): computed solution.

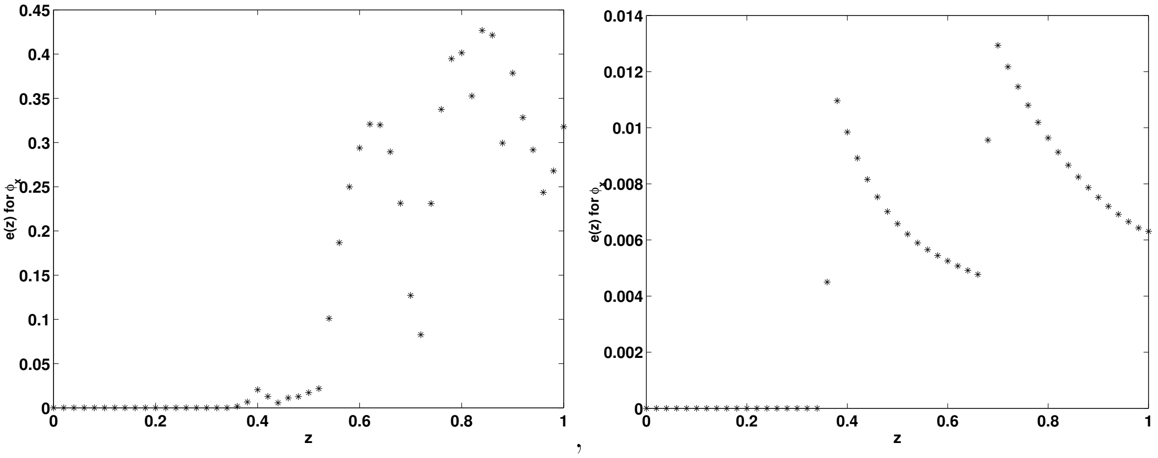

FIG. 7. Relative errors in ϕ_x. Left: fixed grid, maximum relative error is almost 45 percent. Right: adaptive grid, maximum relative error is less than 1.5 percent.

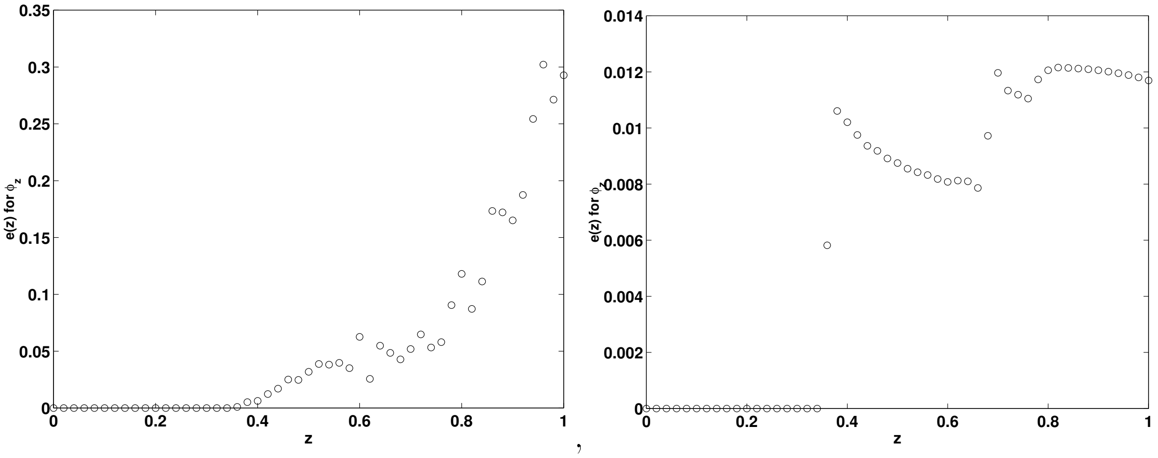

FIG. 8. Relative errors in ϕ_z. Left: fixed grid, maximum relative error is almost 30 percent. Right: adaptive grid, maximum relative error is less than 1.5 percent.

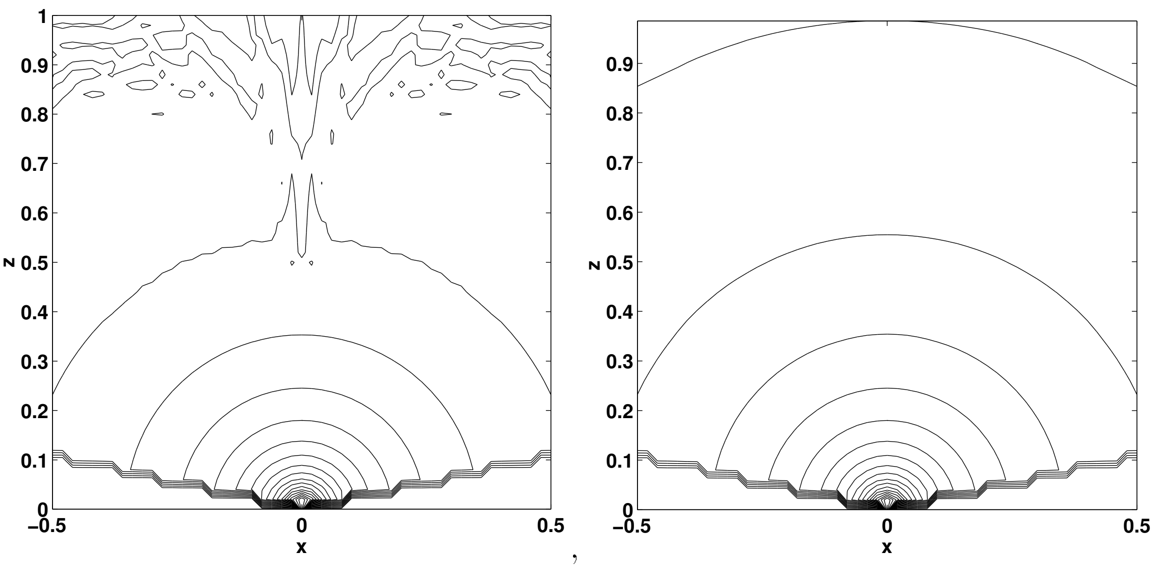

FIG. 9. 2-D amplitude with line source for a constant velocity model. Left: the amplitude by fixed grid is divergent. Right: the amplitude by adaptive grid is convergent.

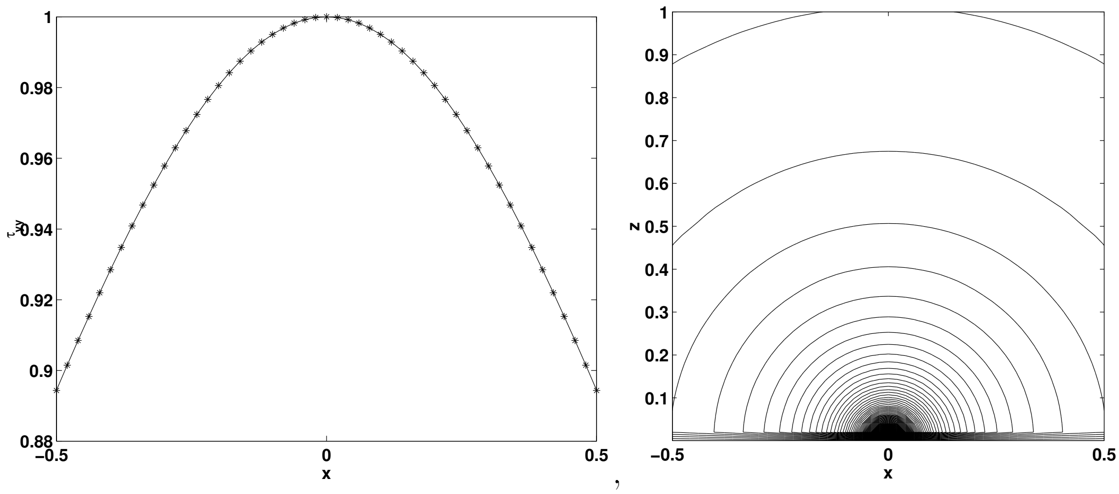

FIG. 10. Left: τ_{yy} at $z = 1$ for a constant velocity model by adaptive grid; solid line (-): true solution; star (*): computed solution. Right: 2D amplitude with point source for a constant velocity model by adaptive grid.

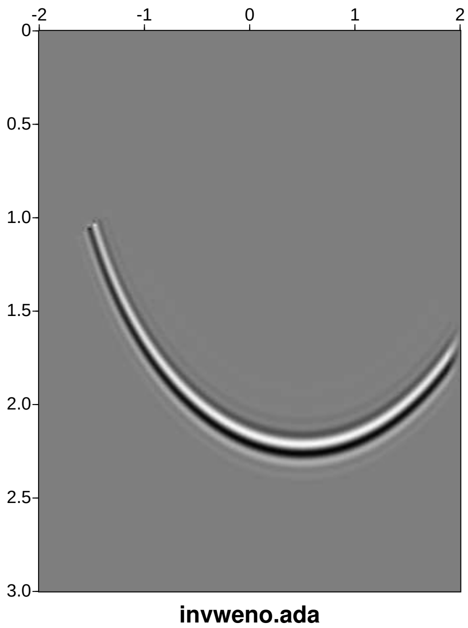

FIG. 11. The impulse response by inversion with adaptive-gridding WENO traveltime-amplitude solver. The Beylkin determinant needed in the inversion is computed by using the information from traveltimes and takeoff angles, and the response is smooth as expected.